Zirconate Pyrochlore Frustrated Magnets: Crystal Growth by the Floating Zone Technique

Monica Ciomaga Hatnean [1], Claudia Decorse [2], Martin R. Lees [1], Oleg A. Petrenko [1] and Geetha Balakrishnan [1,*]

[1] Department of Physics, University of Warwick, Coventry, CV4 7AL, UK; M.Ciomaga-Hatnean@warwick.ac.uk (M.C.H.); M.R.Lees@warwick.ac.uk (M.R.L.); O.Petrenko@warwick.ac.uk (O.A.P.)

[2] SP2M-ICMMO, UMR 8182, Universite Paris-Sud 11, F-91405 Orsay, France; claudia.decorse@u-psud.fr

[*] Correspondence: G.Balakrishnan@warwick.ac.uk; Tel.: +44-247-657-3879

Abstract: This article reviews recent achievements on the crystal growth of a new series of pyrochlore oxides—lanthanide zirconates, which are frustrated magnets with exotic magnetic properties. Oxides of the type $A_2B_2O_7$ (where A = Rare Earth, B = Ti, Mo) have been successfully synthesised in single crystal form using the floating zone method. The main difficulty of employing this technique for the growth of rare earth zirconium oxides $A_2Zr_2O_7$ arises from the high melting point of these materials. This drawback has been recently overcome by the use of a high power Xenon arc lamp furnace for the growth of single crystals of $Pr_2Zr_2O_7$. Subsequently, large, high quality single crystals of several members of the zirconate family of pyrochlore oxides $A_2Zr_2O_7$ (with A = La $\rightarrow$ Gd) have been grown by the floating zone technique. In this work, the authors give an overview of the crystal growth of lanthanide zirconates. The optimum conditions used for the floating zone growth of $A_2Zr_2O_7$ crystals are reported. The characterisation of the crystal boules and their crystal quality is also presented.

Keywords: single crystal growth; floating zone technique; lanthanide zirconate; pyrochlore; fluorite; frustrated magnets

1. Introduction

Pyrochlore oxides have been the subject of extensive investigations due to their fascinating magnetic properties, such as spin ice [1,2], spin glass [3,4], spin liquid [5], or long-range magnetic ordered states [6]. Pyrochlores, compounds of the type $A_2B_2O_7$ (where A = Rare Earth, B = Transition Metal), are a class of frustrated magnets, in which the frustration arises from the arrangement of the magnetic ions (A and/or B ions) in the lattice [6–8]. Both the rare-earth atoms occupying the A sites and the transition metal elements located on the B sites form a three-dimensional network of corner-sharing tetrahedra (see Figure 1), known to display the highest degree of geometrical frustration [6]. In addition, the pyrochlore structure is widely known and studied due to its versatility. Subramanian et al. have shown a wide array of elements (both for the A and B sites) which form the $A_2B_2O_7$ pyrochlore phase [9]. The stability field diagram established by Subramanian et al. reveals that the formation and stability of the pyrochlore oxides is determined by the ionic radii of the constituent ions, or the ionic radius ratio RR = ($r_{A^{3+}}/r_{B^{4+}}$), of $A_2B_2O_7$ and the position of the oxygen ions in the lattice [9].
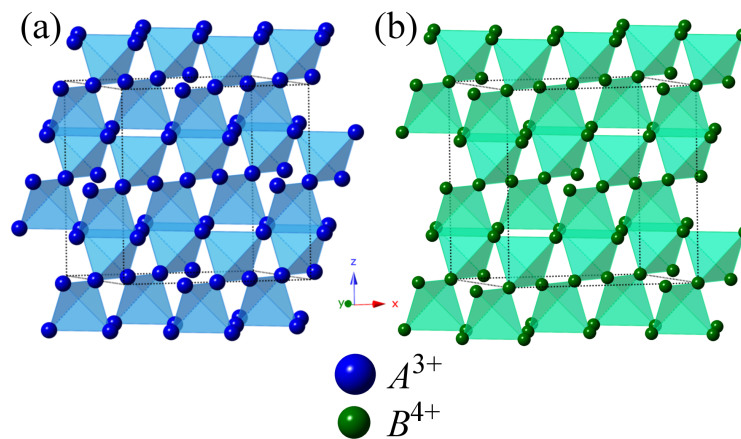
Figure 1. Three-dimensional network of corner-sharing tetrahedra of the *A* (**a**) and *B* site (**b**) sublattices of the pyrochlore structure.

Significant progress has been made in the past decades in the study of the pyrochlore class of frustrated magnets due to breakthroughs in the availability of large, high quality single-crystals of various pyrochlore oxides. Large single crystals of the rare-earth titanate pyrochlores A_2^{3+}Ti$_2$O$_7$ (where A = Pr, Nd, Sm, Tb, Dy, Ho, Er, Y) were grown for the first time by the floating zone technique [10,11]. Following this, crystals of other members of rare earth titanate A_2Ti$_2$O$_7$ (A = Pr → Lu) [12–15] and rare earth molybdate A_2Mo$_2$O$_7$ (where A = Nd, Sm, Gd, Tb, Dy) [16,17] series were prepared using the same technique.

Recent studies have pointed out that strong quantum fluctuations and spin ice correlations may coexist at finite temperature in some pyrochlore materials, due to a reduced magnetic moment on the rare earth A site [18,19]. One of the most exciting areas of future research is into the pyrochlore systems which exhibit this intriguing magnetic ground state (quantum spin liquid) [19]. Reports that propose Pr$_2$Zr$_2$O$_7$ as a candidate material which could display quantum effects [19,20] have motivated researchers to embark upon the study of the zirconate pyrochlore series, A_2Zr$_2$O$_7$ (with A = La → Gd).

There have been several reports on investigations of polycrystalline samples of A_2Zr$_2$O$_7$ (see References [21,22] and references therein). A recent study of the Pr$_2$Zr$_2$O$_7$ pyrochlore demonstrated the feasibility of producing large crystals of this frustrated magnet [23], and pointed to the possibility of producing crystals of other members of the rare earth zirconate pyrochlore oxides by the floating zone technique. Single crystals of several members of the A_2Zr$_2$O$_7$ (with A = La → Gd) family have since been successfully obtained [20–22,24].

2. Factors Affecting Crystal Growth

The main difficulties that have hampered the crystal growth of A_2Zr$_2$O$_7$ pyrochlore oxides by the floating zone technique are described in the following sections.

2.1. High Melting Point

Lanthanide zirconate oxides A_2Zr$_2$O$_7$ have a high melting point and until recently, it has proven difficult to obtain crystals of these materials [25]. A study of the phase diagram of A_2O$_3$-ZrO$_2$ (where A = La and Nd) reports the pyrochlore type oxides melt congruently above 2000 °C [25]. Crystals of the zirconate pyrochlores family can therefore be grown by the floating zone technique, but the optical furnaces used for this purpose have to be able to reach temperatures above 2000 °C. The crystal growth can thus be carried out only with an optical furnace equipped with high power Xenon arc lamps, capable of achieving temperatures up to 2800 °C.

2.2. Evaporation

Among the lanthanide zirconate oxides, evaporation losses during the crystal growth process occur only in the case of $Pr_2Zr_2O_7$. Matsuhira et al., in their first report on the crystal growth of $Pr_2Zr_2O_7$, report the evaporation of Pr_2O_3 during the synthesis [23]. Consequently, the grown boules of $Pr_2Zr_2O_7$ show a reduced Pr content. The magnetic behaviour of this system is directly dependent on the Pr/Zr site occupancy/ratio; thus, it is crucial to minimise any change in stoichometry and to determine accurately the cationic content of the $Pr_2Zr_2O_7$ crystals [20,21,24]. Cationic or anionic vacancies and/or site mixing of Pr/Zr could modify the magnetic response of the system [21,24].

2.3. Mixed Valence State

Recent studies [21,24] report on the existence of mixed valence praseodymium in the $Pr_2Zr_2O_7$ crystals. The inclusion of small amounts of Pr^{4+} can be easily identified by visual inspection of the crystal boules. $Pr_2Zr_2O_7$ crystals that contain even a very small quantity of Pr^{4+} are brown coloured. When these crystals are annealed in a reducing atmosphere (Ar + 3%H_2) at 1200 $°C$ for 2 days, the crystals become bright green coloured (see Reference [21] and references therein). The change in colour is associated with a change of the oxidation state of the Pr^{4+} ions to Pr^{3+}. Koohpayeh et al. report that the Pr^{4+}/Pr^{3+} content ratio can be controlled by performing the floating zone crystal growth in argon atmosphere; thus the 3+ state of praseodymium is favoured over the 4+ oxidation state [24].
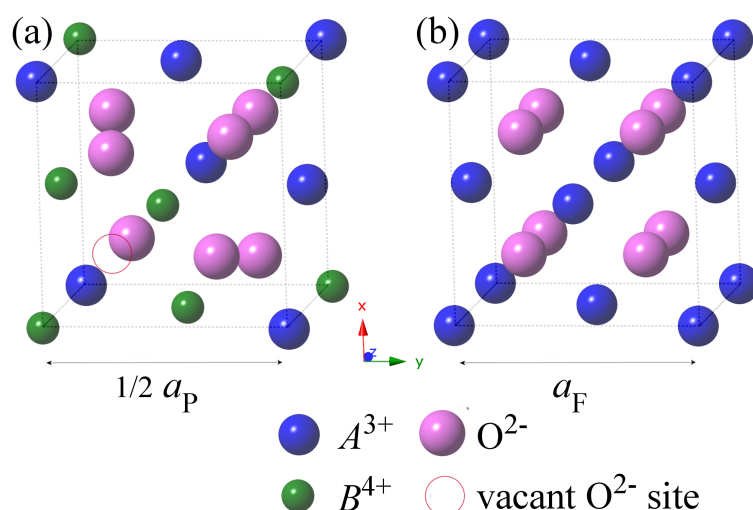
2.4. Crystal Structure

At room temperature and at ambient pressures, lanthanide zirconium oxides $A_2Zr_2O_7$ (with A = La → Lu) crystallize in the cubic system. Furthermore, the crystal structure of $A_2Zr_2O_7$ can be stabilized with one of two different space groups ($Fd\bar{3}m$ and $Fm\bar{3}m$), depending on the ionic radius ratio of the two metallic ions, RR = $\left(r_{A^{3+}}/r_{Zr^{4+}}\right)$.

Lanthanide zirconium oxides $A_2Zr_2O_7$ containing small lanthanide elements (with A = Tb → Lu) (see Table 1), with the ionic radius ratio, RR, ranging from 1.44 to 1.36, crystallize in a defect-fluorite structure (space group $Fm\bar{3}m$ (No. 225)) [9]. Compounds $A_2Zr_2O_7$ formed with larger lanthanides ions (where A = La → Gd), with the ionic radius ratio, RR, ranging from 1.61 to 1.46, adopt the cubic pyrochlore structure (space group $Fd\bar{3}m$ (No. 227)) [9].

Table 1. Effective ionic radii [26] of lanthanides and zirconium ions and the calculated ionic radius ratio RR = $\left(r_{A^{3+}}/r_{Zr^{4+}}\right)$ of the constituent ions of $A_2Zr_2O_7$ (with A = La → Lu).

Ion	Coordination Number	Effective Ionic Radius (Å)	RR = $\left(r_{A^{3+}}/r_{Zr^{4+}}\right)$
La^{3+}	8	1.16	1.61
Pr^{3+}	8	1.126	1.56
Pr^{4+}	8	0.96	—
Nd^{3+}	8	1.109	1.54
Sm^{3+}	8	1.079	1.50
Eu^{3+}	8	1.066	1.48
Gd^{3+}	8	1.053	1.46
Tb^{3+}	8	1.04	1.44
Tb^{4+}	8	0.88	—
Dy^{3+}	8	1.027	1.43
Ho^{3+}	8	1.015	1.41
Er^{3+}	8	1.004	1.39
Tm^{3+}	8	0.994	1.38
Yb^{3+}	8	0.985	1.37
Lu^{3+}	8	0.977	1.36
Zr^{4+}	6	0.72	—
Zr^{4+}	8	0.84	—

From a crystallographic point of view, the pyrochlore structure is closely related to the fluorite structure (see Figure 2), except that the former contains two different cation sites and one-eighth of the anions are absent, and therefore, the coordination of one of the cation sites is reduced from eight to six [27]. The large trivalent rare-earth A^{3+} ions occupy the eight-fold oxygen coordinated A sites, while the six-fold coordinated sites are filled by the smaller tetravalent transition metal ions B^{4+} [9]. In conclusion, the pyrochlore structure could be described as an anion-deficient, cation-ordered derivative ($A_2B_2O_7$) of the fluorite structure type (A_4O_8). One of the key signatures of cation-ordering in the pyrochlore structure is the appearance of superlattice peaks in a diffraction pattern and these can be observed in the X-ray profiles.

Figure 2. (**a**) The pyrochlore crystal structure is shown as a derivative of the fluorite structure; (**b**) For comparison, the unit cell of the fluorite lattice is depicted.

At high temperature ($T > 1500\,^\circ$C), lanthanide zirconate oxides $A_2Zr_2O_7$ (where A = Nd → Gd) undergo an order-disorder transition from a pyrochlore to a defect-fluorite structure. The transition temperature depends on the nature of the rare-earth ion [9,28–30]. Therefore, lanthanum zirconate exists only in the pyrochlore form, whereas for neodymium, samarium, and the gadolinium zirconates, a transition from a pyrochlore to a defect-fluorite structure occurs on heating at 2300, 2000, and 1530 $^\circ$C respectively [28].

Table 2. Summary of the reported structural phase transition temperatures and melting points of some $A_2Zr_2O_7$ oxides. The order to disorder transformation temperatures were either obtained experimentally [28,31] or predicted by calculations [30]. A large number of phase diagrams can be found in the literature for the ZrO_2 - A_2O_3 systems and the published results vary considerably, however the melting temperatures in all cases are reported to be higher than 2000 $^\circ$C for the $A_2Zr_2O_7$ oxides. The melting points were obtained from measurements [25,32,33] and/or estimated from calculations of the phase diagrams [25,34].

Chemical Composition	Pyrochlore ↔ Defect-Fluorite Transition Temperature ($^\circ$C)	Data Acquisition	Melting Point ($^\circ$C)
$La_2Zr_2O_7$	—	—	2100–2350 [25,32,33]
$Pr_2Zr_2O_7$	—	—	2300 [32]
$Nd_2Zr_2O_7$	2300	experiment [28,31]	2300–2350 [25,32]
$Sm_2Zr_2O_7$	2000	experiment [28]	2350 [32]
$Gd_2Zr_2O_7$	1530	experiment [28]	2570 [34]
$Tb_2Zr_2O_7$	~1350	prediction [30]	—

The order disorder transition occurs at 2300 °C and at 2000 °C for the $Nd_2Zr_2O_7$ and $Sm_2Zr_2O_7$ oxides, respectively [28,31]. Therefore, it could prove difficult to prepare single crystals of these materials with a pyrochlore structure, due to the relatively small difference between the melting point and the structural transition temperature (see Table 2 and References [25,28]). A key step in the growth of these materials is to determine their crystallographic structure, to customise and establish the optimum conditions of synthesis to obtain the desired crystal phase [22,31,35].

Furthermore, in the $Gd_2Zr_2O_7$ system, the order to disorder transition occurs at a lower temperature (1530 °C [28]) than the melting point (See Table 2). The synthesis of crystals of gadolinium zirconate with a pyrochlore structure can therefore prove to be very challenging [22]. Our initial study suggested that single crystals of the gadolinium zirconate can be obtained only in the defect-fluorite structure [22]. We show, however, in the present work that, through a long annealing process, the $Gd_2Zr_2O_7$ crystals undergo a structural transformation from defect-fluorite to pyrochlore structure (see Section 4.2.5).

In addition to the structural phase transition occurring at high temperature, recent studies have shown that the lanthanide zirconate with a pyrochlore structure are not stable at high pressure and that they undergo a pressure induced structural transformation leading to either a monoclinic phase (space group $P2_1/c$) [36,37], or a defect cotunnite-type structure (space group *Pnma*) [38].

3. Methods

In all our work, the starting materials used for the synthesis of the polycrystalline materials were lanthanide oxides, La_2O_3, Pr_6O_{11}, Nd_2O_3, Sm_2O_3, Gd_2O_3 and Tb_4O_7 (all of 99.9% purity), and zirconia, ZrO_2 (99%).

Crystals of the lanthanide zirconium pyrochlore oxides, $A_2Zr_2O_7$ (with $A = La \rightarrow Gd$), were then grown using a four-mirror Xenon arc lamp (3 kW) optical image furnace (CSI FZ-T-12000-X_VI-VP, Crystal Systems Incorporated, Japan).

Phase composition analysis was carried out using a Panalytical X-ray diffractometer with a Cu $K\alpha_1$ anode ($\lambda = 1.5406$ Å) or a Bruker D5005 X-ray diffractometer using Cu $K\alpha_1$ and $K\alpha_2$ radiation ($\lambda_{K\alpha 1} = 1.5406$ Å and $\lambda_{K\alpha 2} = 1.5444$ Å). The diffraction patterns were collected at room temperature over an angular range of 10 to 110° in 2θ with a step size in the scattering angle 2θ of 0.013° (Panalytical) or 0.02° (Bruker) and at various scanning times. The analysis of the X-ray patterns was performed using the Fullprof software suite [39].

A Laue X-ray imaging system with a Photonic-Science Laue camera was used to investigate the quality of the as-grown and annealed crystal boules and to orient single crystal samples for selected experiments.

4. Floating Zone Growth of $A_2Zr_2O_7$ (with $A = La \rightarrow Gd$)

4.1. Feed Rod Preparation

Samples of $A_2Zr_2O_7$ (with $A = La \rightarrow Tb$) were first prepared in polycrystalline form by the conventional solid state synthesis method. To ensure the appropriate composition of the final compound, the starting reagents were pre-annealed in air at 1000 °C for 24 h. Powders of starting oxide materials were then weighed in stoichiometric amounts, mixed together and heat treated in air for several days (in 3 or 4 steps) at temperatures in the range 1300–1450 °C. The annealed materials were reground between each step of the synthesis to ensure good homogeneity and to facilitate the reaction of the starting materials. The resulting material was then isostatically pressed into rods (typically 6–8 mm diameter and 70–80 mm long) and sintered at 1450–1600 °C in air for several days. In the case of $Gd_2Zr_2O_7$, two different samples were prepared and sintered in different conditions. A first set of polycrystalline material (GZO_1) was heated in air below the structural transition temperature (following the procedure described in Reference [40]), while the second batch (GZO_2) was prepared

at a temperature above the transition (1530 °C [28]). A summary of the optimum conditions used for sintering the polycrystalline materials is given in Table 3.

Table 3. Summary of the conditions used for the preparation of the $A_2Zr_2O_7$ feed rods. Two samples of $Gd_2Zr_2O_7$ composition were prepared at the different temperatures given below. All the polycrystalline materials were sintered for a duration of 48 to 96 h. The crystal phase of each sample is given, with the corresponding lattice constants.

| Chemical Composition	Sample Label	Sintering Temperature (°C)	Space Group Structure-Type	Lattice Parameter (Å) Present Work	Literature
$La_2Zr_2O_7$	LZO	1550	$Fd\bar{3}m$ (Pyrochlore)	10.8115(1)	10.805 [9]
$Pr_2Zr_2O_7$	PZO	1500	$Fd\bar{3}m$ (Pyrochlore)	10.7098(1)	10.715 [9]
$Nd_2Zr_2O_7$	NZO	1500	$Fd\bar{3}m$ (Pyrochlore)	10.6751(1)	10.678 [9]
$Sm_2Zr_2O_7$	SZO	1500	$Fd\bar{3}m$ (Pyrochlore)	10.5984(1)	10.594 [9]
$Gd_2Zr_2O_7$	GZO_1	1450	$Fd\bar{3}m$ (Pyrochlore)	10.4988(1)	10.528 [9]
$Gd_2Zr_2O_7$	GZO_2	1600	$Fm\bar{3}m$ (Defect-fluorite)	5.2737(1)	5.2636(1) [41]
$Tb_2Zr_2O_7$	TZO	1600	$Fm\bar{3}m$ (Defect-fluorite)	5.2260(1)	5.225 [42]

Room temperature powder X-ray diffraction measurements were performed to determine the phase purity of the polycrystalline material. The X-ray diffraction patterns (see Figure 3) reveal that the $Fd\bar{3}m$ pyrochlore-type structure is formed for LZO, PZO, NZO, SZO and GZO_1, whereas the GZO_2 and TZO samples show a $Fm\bar{3}m$ defect-fluorite-type structure. In all the synthesised materials, no unindexed reflections were observed in the X-ray profiles of the polycrystalline material.

The lattice parameters of the $A_2Zr_2O_7$ samples with a pyrochlore structure were found to be in agreement with the previously reported values for polycrystalline materials [9,41,42], except for GZO_1. The small difference of the lattice constant could be explained by small variations of the stoichiometry or by the presence of a small amount of disorder in this sample (for instance, a coexistence of the pyrochlore and defect-fluorite structures). This hypothesis could be confirmed by further high resolution diffraction experiments that will allow us to establish the site occupancy factors.

In an attempt to obtain the pyrochlore phase of $Tb_2Zr_2O_7$, the polycrystalline material was subsequently annealed in air at temperatures in the range 1000 to 1300 °C for several days (below the predicted structural phase transition temperature of 1350 °C [30]), and slowly cooled to room temperature at rates of 25 to 50 °C/h. X-ray diffraction measurements were then carried out and the results show that even after a long annealing process followed by slow cooling to room temperature, there is no evidence of a disorder to order transformation of $Tb_2Zr_2O_7$. Subsequently, the structure of $Tb_2Zr_2O_7$ is, therefore, best described as a defect-fluorite with the formula $Tb_{0.5}Zr_{0.5}O_{1.75}$ (see the comparison between the pyrochlore and the fluorite structure in the Section 2.4). No crystal growth of this material was attempted due to the lack of success in preparing the desired pyrochlore phase.

4.2. Crystal Growth Details

Crystals of the lanthanide zirconate, $A_2Zr_2O_7$ (with A = La → Gd), were grown by the floating zone method. A snapshot of the crystal growth of a boule of $Pr_2Zr_2O_7$ is shown in Figure 4. Initially, polycrystalline rods were used as seeds and once good quality crystals were obtained, a crystal seed was used for subsequent growths. The two rods (feed and seed) were counter-rotated at a rate of 20–30 rpm. X-ray Laue patterns taken along the lengths and cross sections of the crystals grown indicated that, although the first few millimetres of the crystal boules were of good crystalline quality, some changes of orientation were observed and several different grains could be identified. However, as the crystal growth progressed, the remaining section of each crystal boule obtained was of homogeneous high crystalline quality. In the following sections, we give an outline of the crystal growth conditions of each lanthanide zirconate. The results were previously published in References [21,22].
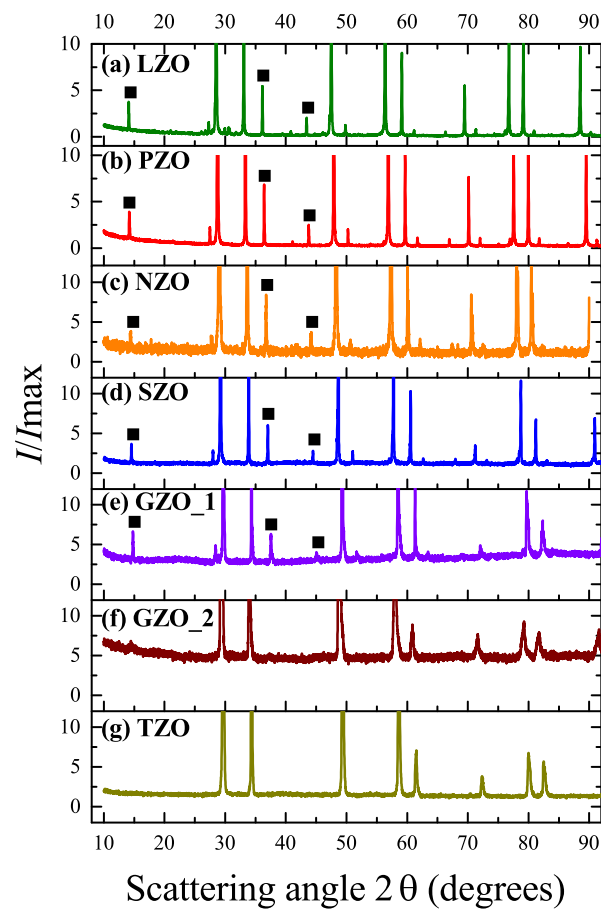
Figure 3. (**a–g**) Room temperature X-ray diffraction patterns of polycrystalline samples of $A_2Zr_2O_7$ (with A = La → Tb) plotted to show the low intensity Bragg peaks. The experimental profiles are given in relative intensities as a function of the scattering angle 2θ. LZO (**a**); PZO (**b**); NZO (**c**); SZO (**d**); and GZO_1 (**e**) samples have a cubic $Fd\bar{3}m$ pyrochlore structure ("■" indicate the low angle superlattice reflections of the pyrochlore structure). GZO_2 (**f**) and TZO samples (**g**) crystallize in the cubic $Fm\bar{3}m$ defect-fluorite structure. The two $Gd_2Zr_2O_7$ samples were prepared using the different synthesis conditions given in Table 3.
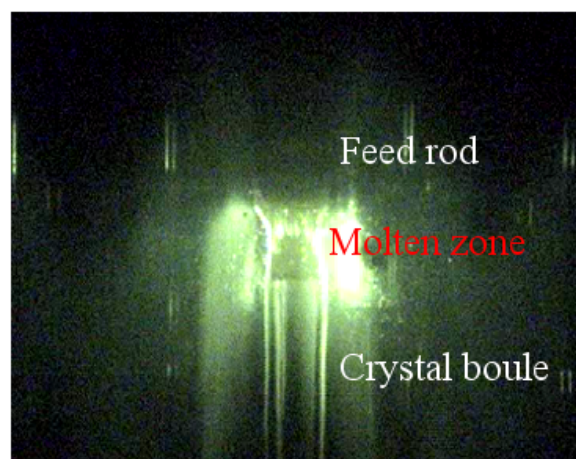
Figure 4. Floating zone growth of a boule of $Pr_2Zr_2O_7$ in air at a growth rate of 12.5 mm/h.
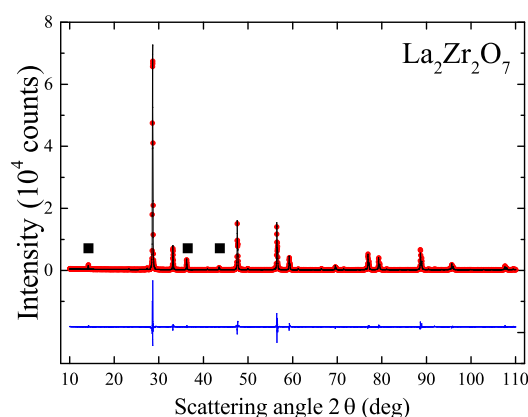
4.2.1. La$_2$Zr$_2$O$_7$

Lanthanum zirconate crystals were grown by the floating zone technique using growth rates in the range 10 to 15 mm/h. No evaporation was observed for any of the growths. The La$_2$Zr$_2$O$_7$ boules were typically 5 to 7 mm in diameter and measured between 30 to 50 mm in length. The crystals developed facets as they grew and two very strong facets were present on almost the entire length of most of the grown crystals. All the lanthanum zirconate boules were transparent to light and colourless. Figure 5e shows a photograph of a crystal of La$_2$Zr$_2$O$_7$, which was grown in air at a growth speed of 15 mm/h. The quality of the grown boules was investigated by X-ray Laue diffraction, and Laue photographs were taken along the length of the boule, on the faceted sides (see Figure 5a–d). The Laue patterns were identical along the whole length of the faceted faces and in most cases, the [100] direction is almost orthogonal to one of the facets. Laue patterns were also taken at several positions along the cross section of the boule at ∼15 mm from the beginning of the boule. The Laue photographs were consistent with one another (see Figure 5f) and showed that the crystal growth direction was only a few degrees away from the [100] direction.
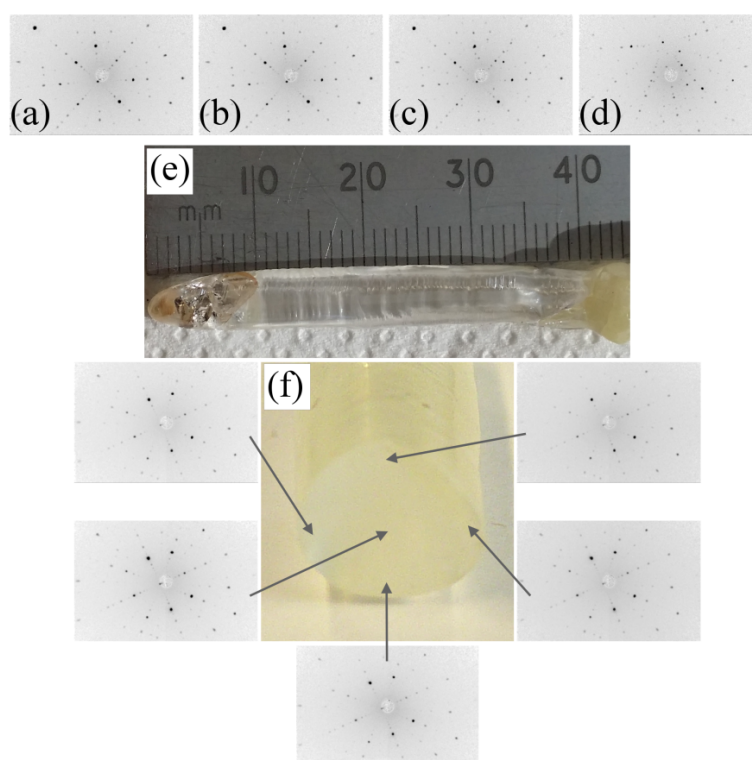
Figure 5. (**a–d**) X-ray Laue back reflection photographs of one of the facets of a La$_2$Zr$_2$O$_7$ crystal, taken along the crystal length at ∼12 mm intervals, between the end (left) and the beginning (right) of the boule. The corresponding Laue patterns taken on the facet at 180 degrees are mirror images of these patterns; (**e**) Boule of La$_2$Zr$_2$O$_7$ prepared by the floating zone method in air at a growth rate of 15 mm/h; (**f**) Laue patterns taken of the cross section of the boule at ∼15 mm from the beginning of the boule, are consistent with one another at several points covering the entire surface. Five patterns corresponding to scans across the diameter of the boule, taken at ∼2 mm intervals, are shown.

The powder X-ray diffraction profile of a ground portion of a single crystal of La$_2$Zr$_2$O$_7$ (grown in air at a growth rate of 15 mm/h) is shown in Figure 6. The pattern reveals the presence of some low-angle weak superlattice reflections (with (*hkl*) = (111), (331), and (511)), which are a key feature of the cation-ordering in the pyrochlore-type structure. All the peaks observed were indexed in the cubic $Fd\bar{3}m$ space group, and no impurity peaks were observed in the patterns. The lattice parameter of the powdered La$_2$Zr$_2$O$_7$ crystal was found to be 10.7992(1) Å [22].

Figure 6. Room temperature powder X-ray diffraction pattern of a ground $La_2Zr_2O_7$ crystal grown in air at a growth rate of 15 mm/h. The experimental profile (red closed circles) and a full profile matching refinement (black solid line) made using the $Fd\bar{3}m$ cubic structure are shown, with the difference given by the blue solid line. "■" indicate the low angle superlattice reflections of the pyrochlore structure.
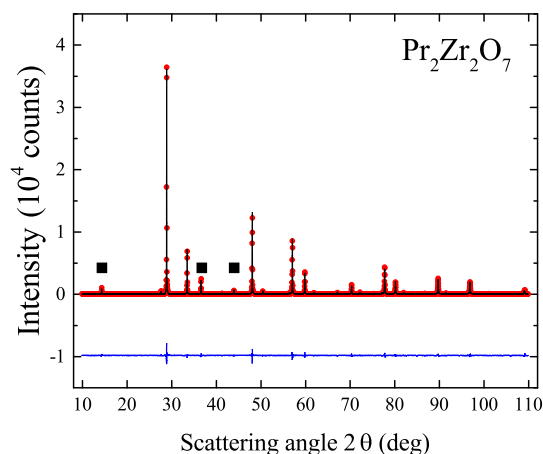
4.2.2. $Pr_2Zr_2O_7$

Crystal growths of $Pr_2Zr_2O_7$ were carried out in various atmospheres, at speeds in the range 10 to 15 mm/h. A brown coloured deposition was observed on the quartz tube surrounding the feed and seed rods, indicating the evaporation of Pr_2O_3 during the growth process. The crystal boules grown in air and in oxygen at pressures in the range 1 to 4 bars were transparent to light, with a dark brown colour (see Figure 7e). As-grown crystals were annealed in a reducing atmosphere (Ar + 3%H_2) at 1200 °C for 2 days, and the crystals become bright green coloured. The crystal growth carried out in argon at a pressure of 1 bar yielded crystal boules with a bright green colour (see Figure 7f). Regardless of the growth conditions, the crystals obtained were typically 5 to 8 mm in diameter and 40 to 85 mm long. The crystals developed facets as they grew and two very strong facets were present on almost the entire length of most of the crystals. Laue patterns taken of one of the facets indicate that the [111] direction is nearly orthogonal to the facet. The Laue photographs were consistent for almost the whole length of the crystal boule (see Figure 7a–d).

Room temperature powder X-ray diffraction data were collected on small portions of the crystals that were ground. The XRD results show that, regardless of the growth conditions used (either followed by post-annealing or not), the $Pr_2Zr_2O_7$ crystals obtained are of the pure pyrochlore structure (see Figure 8 for the crystal grown in air at a growth rate of 12.5 mm/h). The lattice parameter was found in this case to be equal to 10.7010(1) Å. The lattice characteristics, such as lattice constant, site mixing of Pr/Zr, cationic or anionic vacancies, are sample dependent (see References [20,21,24] for detailed structural analysis), and it is thus important to investigate in detail the crystal structure of each sample. To ascertain the cationic Pr/Zr ratio and to investigate the anionic deficiency of the crystals, single crystal X-ray and neutron diffraction experiments were carried out (the results are discussed elsewhere [21]). The stoichiometry in our crystals was found to be close to the ideal pyrochlore composition (2:2:7).
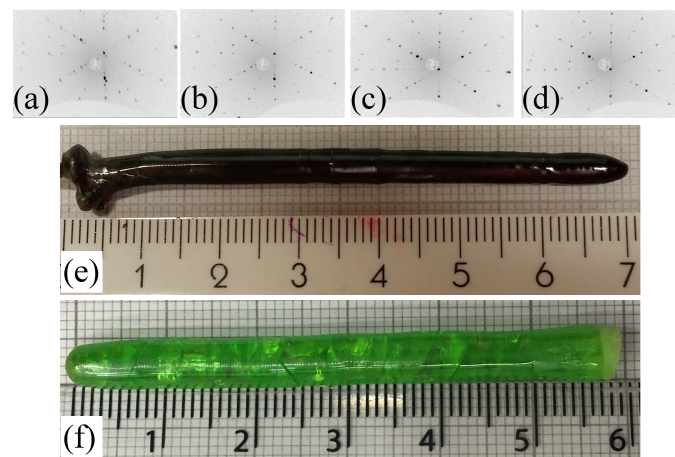
Figure 7. (**a**–**d**) Laue photographs of one of the facets of a $Pr_2Zr_2O_7$ crystal, taken along the crystal length at ∼15 mm intervals, between the beginning (left) and the end (right) of the boule shown in (**e**). The corresponding Laue patterns taken on the facet at 180 degrees are mirror images of these patterns. (**e**) Boule of $Pr_2Zr_2O_7$ prepared by the floating zone method in air at a growth rate of 12.5 mm/h. (**f**) Boule of $Pr_2Zr_2O_7$ prepared by the floating zone method in argon, at 1 bar pressure and using a growth rate of 12.5 mm/h.


Figure 8. Room temperature powder X-ray diffraction pattern of a ground boule of $Pr_2Zr_2O_7$ prepared in air at a growth rate of 12.5 mm/h. The experimental profile (red closed circles) and a full profile matching refinement (black solid line) to the pyrochlore structure are shown, with the difference given by the blue solid line. "■" indicate the low angle superlattice reflections of the pyrochlore structure.

4.2.3. $Nd_2Zr_2O_7$

Crystals of the neodymium zirconate, $Nd_2Zr_2O_7$, were grown in air, at speeds in the range 10 to 15 mm/h. No evaporation was observed in any of the growths. All the boules were transparent to light, with a dark purple colour. The crystals were typically 5 to 7 mm in diameter and 55 to 65 mm long. The boules tended to have thermally generated cracks in most cases, regardless of the growth rate employed. The crystals developed facets as they grew and two very strong facets were present along almost the entire length of most of the crystals. A photograph of an as-grown crystal of $Nd_2Zr_2O_7$ prepared in air at a rate of 12.5 mm/h, is shown in Figure 9e. Laue back reflection photographs taken along the crystal length confirm the high quality of the grown boules (see Figure 9a–d) and indicate that the [111] direction is nearly orthogonal to the facets seen on the sides of the as-grown crystal boule. Identical patterns were obtained along almost the entire length of the faceted faces.
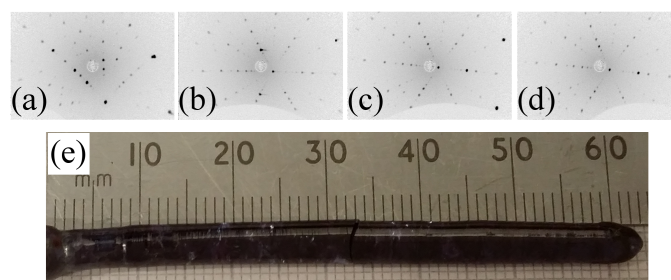
Figure 9. (**a**–**d**) Laue patterns of one of the facets of a $Nd_2Zr_2O_7$ crystal, taken along the crystal length at ~15 mm intervals, between the beginning (left) and the end (right) of the boule. The corresponding Laue patterns taken on the facet at 180 degrees are mirror images of these patterns; (**e**) Crystal of $Nd_2Zr_2O_7$ grown in air at a rate of 12.5 mm/h.

To analyze the microstructure and to investigate the crystal perfection of the floating zone-grown crystals, pieces of the $Nd_2Zr_2O_7$ boules were cut along the growth direction, polished and studied using polarized light microscopy. Polarized light microscopy analysis of the the cross section of the crystal with polished pieces cut from the boule of $Nd_2Zr_2O_7$ shows no evidence of the existence of grain boundaries, suggesting that the boule is monocrystalline. Macroscopic defects (cracks) observed on the crystal boules were probably caused by the large temperature gradient that exists inside the image furnace during the crystal growth.

We also attempted to grow crystals of $Nd_2Zr_2O_7$ in oxygen, at a pressure of 2.5 bars. In this case, the growths were less stable and the resulting boules were of inferior quality.

In order to ascertain the crystal phase attained in our $Nd_2Zr_2O_7$ crystals, powder X-ray diffraction measurements were carried out. An analysis of the pattern provided a good fit to the pyrochlore structure (space group $Fd\bar{3}m$) (see Figure 10). There were no impurity peaks observed in the pattern. The superlattice reflections (with hkl = (111), (331), and (511) characteristic to the pyrochlore structure were observed on the X-ray profiles. The lattice parameter was calculated of a value of 10.6134(1) Å for a $Nd_2Zr_2O_7$ crystal prepared in air at a rate of 12.5 mm/h [22]. Detailed structural investigations of the crystal boules were performed and the results of the room-temperature X-ray diffraction and time-of-flight neutron-scattering experiments show that the crystals are stoichiometric in composition with no measurable site disorder (the results are discussed elsewhere [43]).
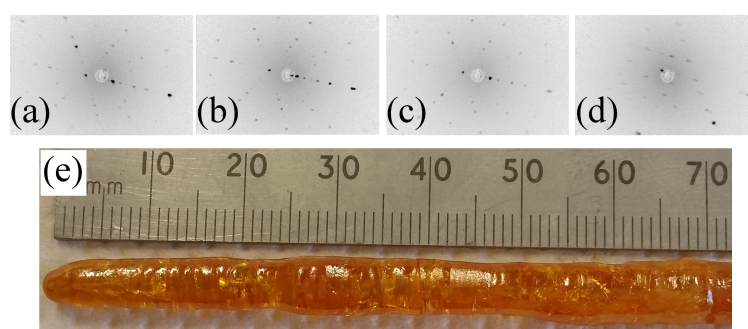
4.2.4. $Sm_2Zr_2O_7$

The crystal growths were carried out in oxygen, at a pressure of 4 bars, using growth rates in the range 5–15 mm/h. No evaporation was observed on the quartz tube surrounding the sample for any of the growths.

The as-grown samarium zirconate crystals were typically 5 to 7 mm in diameter and 30 to 90 mm long. The $Sm_2Zr_2O_7$ boules tended to have cracks which are probably due to the large temperature gradient in the furnace during the crystal growth. The crystals developed facets as they grew and two very strong facets were present along almost the entire length of most of the crystals. The crystal boules have a light orange colour. A photograph of a crystal of $Sm_2Zr_2O_7$, which was grown in oxygen at a pressure of 4 bars and a growth speed of 8 mm/h, is shown in Figure 11e. Figure 11a–d show the X-ray Laue photographs taken of a facet of a boule of $Sm_2Zr_2O_7$. The Laue patterns indicate that the [111] direction is nearly orthogonal to the facets seen on the sides of the as-grown crystal boule.
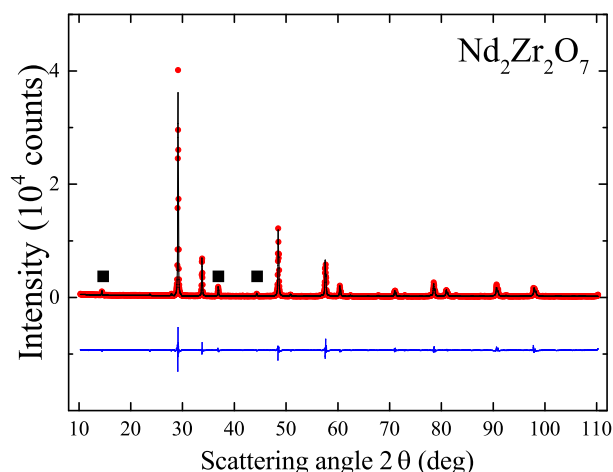
Figure 10. Powder X-ray diffraction pattern collected on a ground boule of $Nd_2Zr_2O_7$ prepared in air at a rate of 12.5 mm/h. The experimental profile (red closed circles) and a full profile matching refinement (black solid line) to the pyrochlore structure are shown, with the difference given by the blue solid line. "■" indicate the low angle superlattice reflections of the pyrochlore structure.

Figure 11. (**a**–**d**) X-ray Laue back reflection photographs of a facet of a $Sm_2Zr_2O_7$ crystal, taken along the crystal length at ∼12 mm intervals, between the end (left) and the beginning (right) of the boule. The corresponding Laue patterns taken on the facet at 180 degrees are mirror images of these patterns; (**e**) Boule of $Sm_2Zr_2O_7$ prepared in oxygen, at 4 bars pressure and using a growth rate of 8 mm/h.

Attempts to prepare single-crystals of $Sm_2Zr_2O_7$ in air proved to be unsuccessful. The growths were unstable and the resulting boules were of poor quality.

Figure 12 shows the room temperature X-ray diffraction profile of a powdered crystal sample of $Sm_2Zr_2O_7$ grown in oxygen, at 4 bars pressure and using a growth rate of 8 mm/h. The results of the refinement were similar to the other members of the zirconates pyrochlore family. The weak superlattice reflections of the cubic $Fd\bar{3}m$ pyrochlore structure are clearly visible on the X-ray diffraction pattern and no impurity peaks were observed. The sharp Bragg peaks suggest that only the pyrochlore phase of $Sm_2Zr_2O_7$ crystal is formed, with a lattice parameter of 10.5907(1) Å [22].
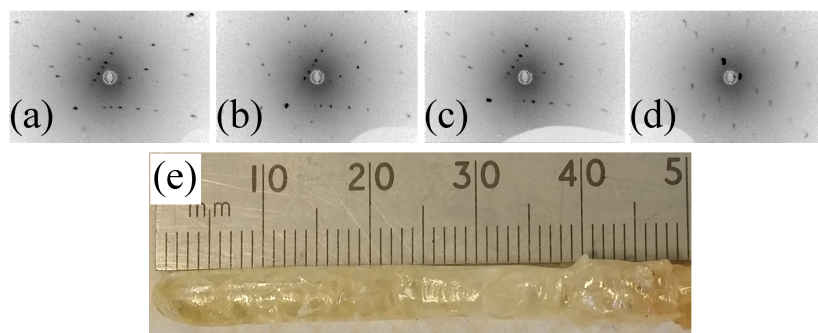
4.2.5. $Gd_2Zr_2O_7$

The starting polycrystalline materials used for the growth of $Gd_2Zr_2O_7$ were the two samples prepared following different synthesis conditions, GZO_1 and GZO_2. The growths of $Gd_2Zr_2O_7$ were performed in air at speeds in the range 10 to 15 mm/h. No evaporation was observed on the quartz tube surrounding the sample during the growth.

The gadolinium zirconate crystal boules grown were typically 5 to 6 mm in diameter and 30 to 40 mm long, and were of light yellow colour. Figure 13e shows a photograph of a crystal of $Gd_2Zr_2O_7$, which was grown in air at a growth rate of 15 mm/h. Not all the crystals had facets. The

X-ray Laue patterns (see Figure 13a–d) indicate that the [111] direction is nearly orthogonal to the facets on the sides of this crystal boule.
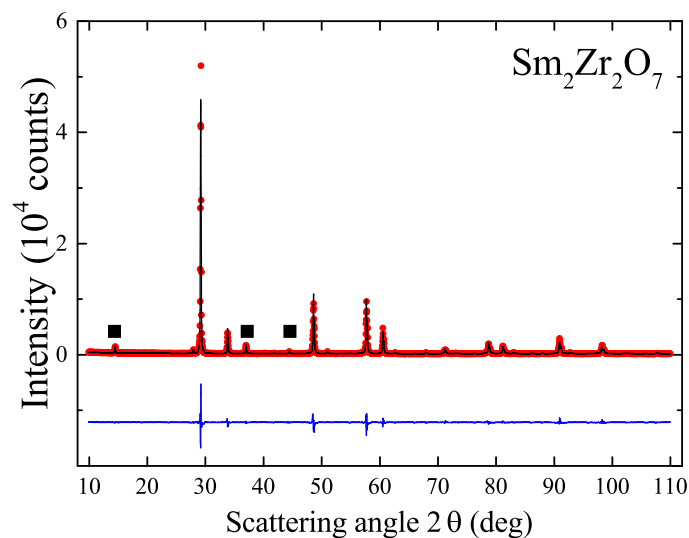
Figure 12. Powder X-ray diffraction profile of a ground crystal of $Sm_2Zr_2O_7$ prepared in oxygen, at 4 bars pressure and using a growth rate of 8 mm/h. The experimental profile (red closed circles) and a full profile matching refinement (black solid line) to the pyrochlore structure are shown, with the difference given by the blue solid line. "■" indicate the low angle superlattice reflections of the pyrochlore structure.


Figure 13. (**a–d**) X-ray Laue back reflection photograph taken on a facet of a crystal of $Gd_2Zr_2O_7$ crystal, taken along the crystal length at ∼10 mm intervals intervals, between the end (left) and the beginning (right) of the boule. The corresponding Laue patterns taken on the facet at 180 degrees are mirror images of these patterns; (**e**) Crystal boule of $Gd_2Zr_2O_7$ prepared in air using a growth rate of 15 mm/h from starting material with the pyrochlore structure, GZO_1.

No evidence of superlattice reflections characteristic of the pyrochlore structure were observed in the X-ray profile of the as-grown $Gd_2Zr_2O_7$ boule (see Figure 14a), and crystals prepared using both the polycrystalline samples, GZO_1 and GZO_2, show identical X-ray diffraction patterns. The data were fitted to the cubic $Fm\bar{3}m$ space group, indicating that the crystal boules of $Gd_2Zr_2O_7$ are obtained only in the defect-fluorite form, with a lattice parameter equal to 5.2614(1) Å [22].

The as-grown $Gd_2Zr_2O_7$ crystals were annealed in air at 1400 °C, a temperature lower than the structural phase transition temperature, for several days, and then slowly cooled to room temperature at a rate of 50 °C/h. No change in colour was observed following the annealing process. The long post-annealing experiments were required to allow the structural transformation from defect-fluorite to pyrochlore, i.e., the cation-ordering which is characteristic of the pyrochlore structure. The results are

confirmed by the X-ray diffraction patterns collected on annealed crystals of $Gd_2Zr_2O_7$ (see Figure 14b). The data were refined against the pyrochlore $Fd\bar{3}m$ structure. The weak superlattice reflections are visible in this case on the X-ray diffraction pattern, indicating that post annealing of the $Gd_2Zr_2O_7$ facilitates the transition to the ordered pyrochlore crystal phase. The lattice parameters for the single crystal sample with the pyrochlore structure (annealed $Gd_2Zr_2O_7$ crystal boule) was found to be equal to 10.5341(1) Å.
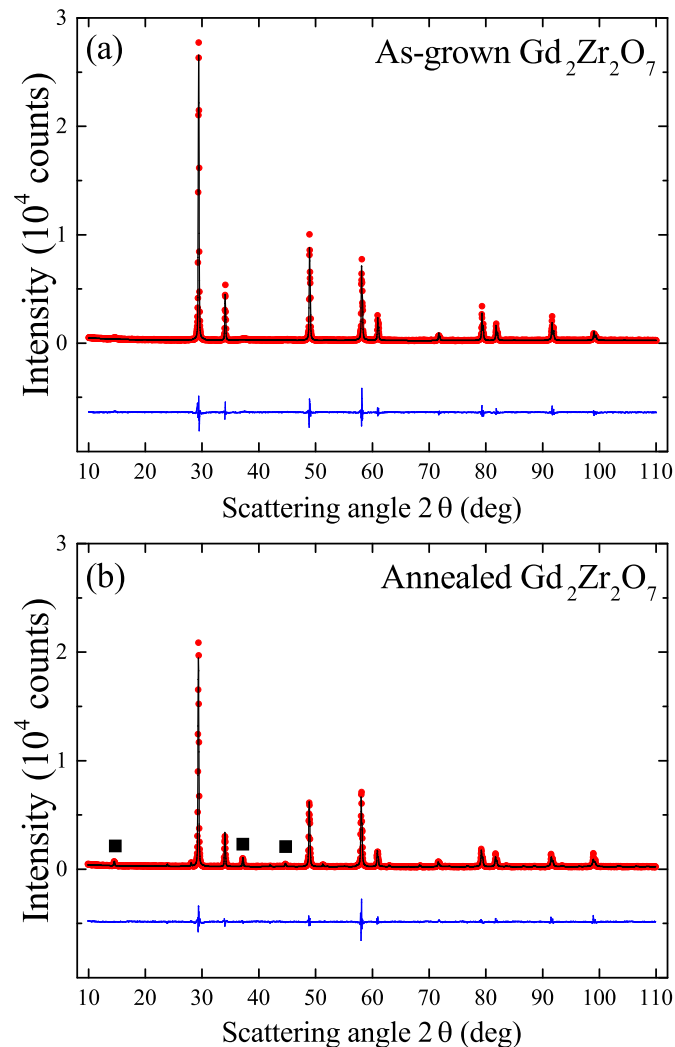
Figure 14. (**a**) Room temperature powder X-ray diffraction pattern collected on an as-grown ground boule of $Gd_2Zr_2O_7$ prepared in air using a growth rate of 15 mm/h from starting material with the pyrochlore structure, GZO_1; (**b**) Powder X-ray diffraction profile of an annealed boule of $Gd_2Zr_2O_7$ (the annealing was carried out in air at 1400 °C for several days). The experimental profile (red closed circles) and a full profile matching refinement (black solid line) to the defect-fluorite (**a**) and pyrochlore (**b**) structures are shown, with the difference given by the blue solid line. "■" indicate the low angle superlattice reflections of the pyrochlore structure.

5. Conclusions

A summary of the crystal growth conditions used for the growth of $A_2Zr_2O_7$ (with $A = La \rightarrow Gd$) is given in Table 4. All the Zr-based pyrochlores appear to melt congruently and little or no evaporation was observed for the growths, except in the case of $Pr_2Zr_2O_7$. The crystal growths were performed using various growth rates and in various atmospheres, nevertheless, crystal boules of $A_2Zr_2O_7$ of large size and better crystal quality were grown using higher growth speeds. The crystal boules of

$A_2Zr_2O_7$ (with A = La → Gd) are very fragile and most of the crystals show a preference to cleave along the [111] direction.

Table 4. Summary of the conditions used for the growth of $A_2Zr_2O_7$ crystals. All the boules grown were transparent to light.

$A_2Zr_2O_7$	Growth rate (mm/h)	Atmosphere	Pressure	Feed and Seed Rotation Rate (rpm)	Remarks
La$_2$Zr$_2$O$_7$	10–15	air	ambient	20–30	colourless boules
Pr$_2$Zr$_2$O$_7$	10–15	air	ambient	20–30	dark-brown boules
	10–15	O$_2$	1–4 bars	20–30	dark-brown boules
	10–15	Ar	1 bar	20–30	bright-green boules
Nd$_2$Zr$_2$O$_7$	10–15	air	ambient	20–30	dark-purple boules
	10–15	O$_2$	2.5 bars	20–30	poor quality boules
Sm$_2$Zr$_2$O$_7$	5–15	O$_2$	4 bars	20–30	light-orange
	5–15	air	ambient	20–30	poor quality boules
Gd$_2$Zr$_2$O$_7$	10–15	air	ambient	20–30	light-yellow
	10–15	O$_2$	1–2 bars	20–30	poor quality boules

The results of the refinements of the room temperature powder X-ray data collected on the $A_2Zr_2O_7$ crystals are listed in Table 5. The lattice parameters for the crystals of the rare earth zirconate oxides family were found to be slightly smaller than the values reported for polycrystalline samples, in both the present work and the literature [9]. The synthesis methods being different, it is possible that the structural characteristics are slightly different. More detailed investigations of the structural parameters through both powder and single crystal diffraction using neutrons/X-rays are necessary in order to determine the A/Zr site occupancy/ratio and/or oxygen deficiencies of the polycrystalline samples in comparison to the single crystal samples.

Table 5. Lattice parameters for $A_2Zr_2O_7$ (with A = La → Gd), refined from the room temperature powder X-ray diffraction data.

Chemical composition		Space Group Structure-Type	Lattice Parameter (Å) Present Work
La$_2$Zr$_2$O$_7$		$Fd\bar{3}m$ (Pyrochlore)	10.7992(1)
Pr$_2$Zr$_2$O$_7$		$Fd\bar{3}m$ (Pyrochlore)	10.7010(1)
Nd$_2$Zr$_2$O$_7$		$Fd\bar{3}m$ (Pyrochlore)	10.6134(1)
Sm$_2$Zr$_2$O$_7$		$Fd\bar{3}m$ (Pyrochlore)	10.5907(1)
Gd$_2$Zr$_2$O$_7$	As-grown	$Fm\bar{3}m$ (Defect-fluorite)	5.2614(1)
Gd$_2$Zr$_2$O$_7$	Annealed	$Fd\bar{3}m$ (Pyrochlore)	10.5341(1)

The growth of large high quality single crystals of this new family of pyrochlore oxides represents a major breakthrough in the field of frustrated magnetism. Single crystal samples of $A_2Zr_2O_7$ (where A = La - Gd) are available from the authors. The availability of crystals of $A_2Zr_2O_7$ lays the foundation for the study of this novel class of pyrochlores, in the quest for frustrated magnets with fascinating properties. Pr$_2$Zr$_2$O$_7$ is a potential candidate for the study of quantum spin liquid states [20], whereas the spin ice candidate Nd$_2$Zr$_2$O$_7$ exhibits antiferromagnetic ordering coexisting with a fluctuating state with ferromagnetic correlations [43–45]. Furthermore, the gadolinium zirconium pyrochlore Gd$_2$Zr$_2$O$_7$ is highly stable under radiation environments and promises to be a suitable host material for nuclear waste immobilization [46].

References

1. Harris, M.J.; Bramwell, S.T.; McMorrow, D.F.; Zeiske, T.; Godfrey, K.W. Geometrical Frustration in the Ferromagnetic Pyrochlore $Ho_2Ti_2O_7$. *Phys. Rev. Lett.* **1997**, *79*, 2554–2557.

2. Ramirez, A.P.; Hayashi, A.; Cava, R.J.; Siddharthan, R.; Shastry, B.S. Zero-Point entropy in 'spin ice'. *Nature* **1999**, *399*, 333–335.

3. Gaulin, B.D.; Reimers, J.N.; Mason, T.E.; Greedan, J.E.; Tun, Z. Spin freezing in the geometrically frustrated pyrochlore antiferromagnet $Tb_2Mo_2O_7$. *Phys. Rev. Lett.* **1992**, *69*, 3244–3247.

4. Gardner, J.S.; Gaulin, B.D.; Lee, S.-H.; Broholm, C.; Raju, N.P.; Greedan, J.E. Glassy Statics and Dynamics in the Chemically Ordered Pyrochlore Antiferromagnet $Y_2Mo_2O_7$. *Phys. Rev. Lett.* **1999**, *83*, 211–214.

5. Gardner, J.S.; Dunsiger, S.R.; Gaulin, B.D.; Gingras, M.J.P.; Greedan, J.E.; Kiefl, R.F.; Lumsden, M.D.; MacFarlane, W.A.; Raju, N.P.; Sonier, J.E.; et al. Cooperative Paramagnetism in the Geometrically Frustrated Pyrochlore Antiferromagnet $Tb_2Ti_2O_7$. *Phys. Rev. Lett.* **1999**, *82*, 1012–1015.

6. Gardner, J.S.; Gingras, M.J.P.; Greedan, J.E. Magnetic pyrochlore oxides. *Rev. Mod. Phys.* **2010**, *82*, 53–107.

7. Ramirez, A.P. Strongly Geometrically Frustrated Magnets. *Annu. Rev. Mater. Sci.* **1994**, *24*, 453–480.

8. Greedan, J.E. Geometrically frustrated magnetic materials. *J. Mater. Chem.* **2001**, *11*, 37–53.

9. Subramanian, M.A.; Aravamudan, G.; Subba Rao, G.V. Oxide Pyrochlores —A Review. *Prog. Solid St. Chem.* **1983**, *15*, 55–143.

10. Gardner, J.S.; Gaulin, B.D.; Paul, D.M.K. Single crystal growth by the floating-zone method of a geometrically frustrated pyrochlore antiferromagnet, $Tb_2Ti_2O_7$. *J. Cryst. Growth* **1998**, *191*, 740–745.

11. Balakrishnan, G.; Petrenko, O.A.; Lees, M.R.; Paul, D.M. Single crystal growth of rare earth titanate pyrochlores. *J. Phys.: Condens. Matter.* **1998**, *10*, L723–L725.

12. Prabhakaran, D.; Boothroyd, A.T. Crystal growth of spin-ice pyrochlores by the floating-zone method. *J. Cryst. Growth* **2011**, *318*, 1053–1056.

13. Chang, L.-J.; Onoda, S.; Su, Y.; Kao, Y.-J.; Tsuei, K.-D.; Yasui, Y.; Kakurai, K.; Lees, M.R. Higgs transition from a magnetic coulomb liquid to a ferromagnet in $Yb_2Ti_2O_7$. *Nat. Commun.* **2012**, *3*, 992.

14. Ross, K.A.; Proffen, T.; Dabkowska, H.A.; Quilliam, J.A.; Yaraskavitch, L.R.; Kycia, J.B.; Gaulin, B.D. Lightly stuffed pyrochlore structure of single-crystalline $Yb_2Ti_2O_7$ grown by the optical floating zone technique. *Phys. Rev. B* **2012**, *86*, 174424.

15. Li, Q.; Xu, L.; Fan, C.; Zhang, F.; Lv, Y.; Ni, B.; Zhao, Z.; Sun, X. Single crystal growth of the pyrochlores $R_2Ti_2O_7$ (*R*=rare earth) by the optical floating-zone method. *J. Cryst. Growth* **2013**, *377*, 96–100.

16. Taguchi, Y.; Ohgushi, K.; Tokura, Y. Optical probe of the metal-insulator transition in pyrochlore-type molybdate. *Phys. Rev. B* **2002**, *65*, 115102.

17. Kézsmárki, I.; Hanasaki, N.; Hashimoto, D.; Iguchi, S.; Taguchi, Y.; Miyasaka, S.; Tokura, Y. Charge dynamics near the electron-correlation induced metal-insulator transition in pyrochlore-type molybdates. *Phys. Rev. Lett.* **2004**, *93*, 266401.

18. Lee, S.; Onoda, S.; Balents, L. Generic quantum spin ice. *Phys. Rev. B* **2012**, *86*, 104412.

19. Gingras, M.J.P.; McClarty, P.A. Quantum spin ice: a search for gapless quantum spin liquids in pyrochlore magnets. *Rep. Prog. Phys.* **2014**, *77*, 056501.

20. Kimura, K.; Nakatsuji, S.; Wen, J.-J.; Broholm, C.; Stone, M.B.; Nishibori, E.; Sawa, H. Quantum fluctuations in spin-ice-like $Pr_2Zr_2O_7$. *Nat. Commun.* **2013**, *4*, 1934.

21. Ciomaga Hatnean, M.; Decorse, C.; Lees, M.R.; Petrenko, O.A.; Keeble, D.S.; Balakrishnan, G. Structural and magnetic properties of single crystals of the geometrically frustrated zirconium pyrochlore, $Pr_2Zr_2O_7$. *Mater. Res. Express* **2014**, *1*, 026109.

22. Ciomaga Hatnean, M.; Lees, M.R.; Balakrishnan, G. Growth of single-crystals of rare-earth zirconate pyrochlores, $Ln_2Zr_2O_7$ (with Ln=La, Nd, Sm, and Gd) by the floating zone technique. *J. Cryst. Growth* **2015**, *418*, 1–6.

23. Matsuhira, K.; Sekine, C.; Paulsen, C.; Wakeshima, M.; Hinatsu, Y.; Kitazawa, T.; Kiuchi, Y.; Hiroi, Z.; Takagi, S. Spin freezing in the pyrochlore antiferromagnet $Pr_2Zr_2O_7$. *J. Phys.: Conf. Ser.* **2009**, *145*, 012031.

24. Koohpayeh, S.M.; Wen, J.-J.; Trump, B.A.; Broholm, C.L.; McQueen, T.M. Synthesis, floating zone crystal growth and characterization of the quantum spin ice $Pr_2Zr_2O_7$ pyrochlore. *J. Cryst. Growth* **2014**, *402*, 291–298.

25. Roth, R.S. Pyrochlore-Type compounds containing double oxides of trivalent and tetravalent ions. *J. Res. Natl. Bur. Stand.* **1956**, *56*, 2643.

26. Shannon, R.D. Revised Effective Ionic Radii and Systematic Studies of Interatomic Distances in Halides and Chaleogenides. *Acta Cryst.* **1976**, *A32*, 751–767.

27. Ewing, R.C.; Weber, W.J.; Lian, J. Nuclear waste disposal —pyrochlore ($A_2B_2O_7$): Nuclear waste form for the immobilization of plutonium and "minor" actinides. *J. Appl. Phys.* **2004**, *95*, 5949–5971.

28. Michel, D.; Jorba, M.P.Y.; Collongues, R. Etude de la transformation ordre-desordre de la structure fluorite a la structure pyrochlore pour des phases $(1 − x)ZrO_2 − xLn_2O_3$. *Mat. Res. Bull.* **1974**, *9*, 1457–1468.

29. Michel, D.; Jorba, M.P.Y.; Collongues, R. Study by raman spectroscopy of order-disorder phenomena occurring in some binary oxides with fluorite- related structures. *J. Raman Spectrosc.* **1976**, *5*, 163–180.

30. Rushton, M.J.D.; Grimes, R.W. Predicted pyrochlore to fluorite disorder temperature for $A_2Zr_2O_7$ compositions. *J. Mater. Res.* **2004**, *19*, 1603–1604.

31. Ohtani, H.; Matsumoto, S.; Sundman, B.; Sakuma, T.; Hasebe, M. Equilibrium between fluorite and pyrochlore structures in the ZrO_2 - Nd_2O_3 system. *Mater. Trans.* **2005**, *46*, 1167–1174.

32. Karaulov, A.G.; Zoz, E.I. Phase formation in the ZrO_2 - HfO_2 - Gd_2O_3 and ZrO_2 - HfO_2 - Yb_2O_3 systems. *B. Acad. Sci. USSR Ch. +* **1966**, *15*, 2011–2016.

33. Radha, A.V.; Ushakov, S.V.; Navrotsky, A. Thermochemistry of lanthanum zirconate pyrochlore. *J. Mater. Res.* **2009**, *24*, 3350–3357.

34. Karaulov, A.G.; Zoz, E.I. Phase formation in the ZrO_2 - HfO_2 - Gd_2O_3 and ZrO_2 - HfO_2 - Yb_2O_3 systems. *Refract. Ind. Ceram.* **1999**, *40*, 479–483.

35. Payne, J.L.; Tucker, M.G.; Evans, I.R. From fluorite to pyrochlore: Characterisation of local and average structure of neodymium zirconate, $Nd_2Zr_2O_7$. *J. Solid State Chem.* **2013**, *205*, 29–34.

36. Kumar, N.R.S.; Shekar, N.V.C.; Sahu, P.C. Pressure induced structural transformation of pyrochlore $Gd_2Zr_2O_7$. *Solid State Commun.* **2008**, *147*, 357–359.

37. Surblé, S.; Heathman, S.; Raison, P.E.; Bouëxière, D.; Popa, K.; Caciuffo, R. Pressure-Induced structural transition in $Ln_2Zr_2O_7$ (Ln = Ce, Nd, Gd) pyrochlores. *Phys. Chem. Minerals* **2010**, *37*, 761–767.

38. Xiao, H.Y.; Zhang, F.X.; Gao, F.; Lang, M.; Ewing, R.C.; Weber, W.J. Zirconate pyrochlores under high pressure. *Phys. Chem. Chem. Phys.* **2010**, *12*, 12472–12477.

39. Rodríguez-Carvajal, J. Recent advances in magnetic structure determination by neutron powder diffraction. *Physica B* **1993**, *192*, 55–69.

40. Blanchard, P.E.R.; Clements, R.; Kennedy, B.J.; Ling, C.D.; Reynolds, E.; Avdeev, M.; Stampfl, A.P.J.; Zhang, Z.; Jang, L.-Y. Does local disorder occur in the pyrochlore zirconates? *Inorg. Chem.* **2012**, *51*, 13237–13244.

41. Moriga, T.; Yoshiasa, A.; Kanamaru, F.; Koto, K.; Yoshimura, M.; Somiya, S. Crystal structure analyses of the pyrochlore and fluorite-type $Zr_2Gd_2O_7$ and anti-phase domain structure. *Solid State Ionics* **1989**, *31*, 319–328.

42. Reynolds, E.; Blanchard, P.E.R.; Kennedy, B.J.; Ling, C.D.; Liu, S.; Avdeev, M.; Zhang, Z.; Cuello, G.J.; Tadich, A.; Jang, L.-Y. Anion Disorder in Lanthanoid Zirconates $Gd_{2−x}Tb_xZr_2O_7$. *Inorg. Chem.* **2013**, *52*, 8409–8415.

43. Ciomaga Hatnean, M.; Lees, M.R.; Petrenko, O.A.; Keeble, D.S.; Balakrishnan, G.; Gutmann, M.J.; Klekovkina, V.V.; Malkin, B.Z. Structural and magnetic investigations of single-crystalline neodymium zirconate pyrochlore $Nd_2Zr_2O_7$. *Phys. Rev. B* **2015**, *91*, 174416.

44. Lhotel, E.; Petit, S.; Guitteny, S.; Florea, O.; Ciomaga Hatnean, M.; Colin, C.; Ressouche, E.; Lees, M.R.; Balakrishnan, G. Fluctuations and All-In—All-Out Ordering in Dipole-Octupole $Nd_2Zr_2O_7$. *Phys. Rev. Lett.* **2015**, *115*, 197202.

45. Petit, S.; Lhotel, E.; Canals, B.; Ciomaga Hatnean, M.; Ollivier, J.; Mutka, H.; Ressouche, E.; Wildes, A.R.; Lees, M.R.; Balakrishnan, G. Observation of magnetic fragmentation in spin ice. *Nat. Phys. Advanced Online Publication* **2016**.

46. Mandal, B.P.; Tyagi, A.K. Pyrochlores: Potential multifunctional materials. *BARC Newsletter* **2010**, *313*, 6–13.